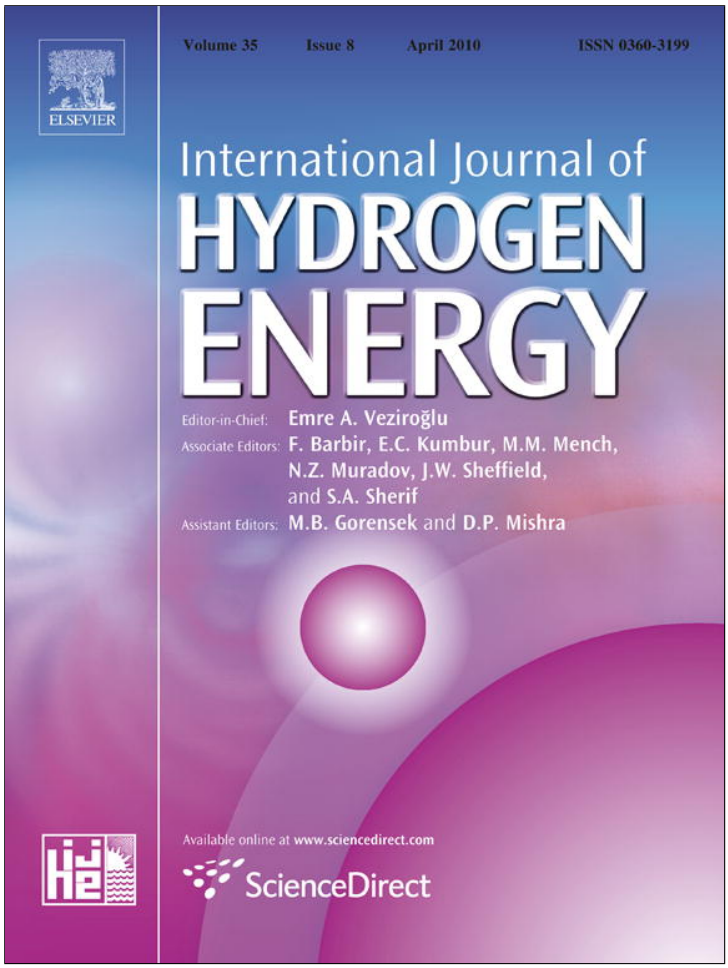

INTERNATIONAL JOURNAL OF HYDROGEN ENERGY 35 (2010) 3472–3479

Available at www.sciencedirect.com

ScienceDirect

journal homepage: www.elsevier.com/locate/he

# A million-channel reformer on a fingertip: Moving down the scale in hydrogen production

*Eduardo López* [a,c,*], *Aitor Irigoyen* [a], *Trifon Trifonov* [b], *Angel Rodríguez* [b], *Jordi Llorca* [a]

[a] *Institut de Tècniques Energètiques, Universitat Politècnica de Catalunya, Diagonal 647, ed. ETSEIB, 08028 Barcelona, Spain*
[b] *Departament d'Enginyeria Electrònica, Universitat Politècnica de Catalunya, Campus Nord, Mòdul C4, c. Jordi Girona 1-3, 08034 Barcelona, Spain*
[c] *Planta Piloto de Ingeniería Química (CONICET-UNS), Camino de la Carrindanga km 7, 8000 Bahía Blanca, Argentina*

ARTICLE INFO

*Article history:*
Received 27 November 2009
Received in revised form
21 January 2010
Accepted 31 January 2010
Available online 3 March 2010

*Keywords:*
Microreactor
Macroporous silicon
Ethanol reforming
Hydrogen

ABSTRACT

The present contribution reports the design, manufacture and experimental proof of concept of an ethanol micro-reformer for portable-fuel cell feeding. Through photo-assisted electrochemical etching, a silicon micromonolithic substrate with perfectly parallel cylindrical channels of 3.3 μm diameter was achieved (density of channels of ca. $4 \times 10^4$ channels $mm^{-2}$). The channel walls were coated with a cobalt-based catalyst. The resultant functionalized micromonoliths were implemented in a stainless steel microreactor including feed evaporation facilities and electrical heating. The unit was successfully tested for ethanol steam reforming under non-diluted feed conditions at 773 K, achieving high hydrogen specific production rates, high ethanol conversions (>80%) and adequate selectivity profiles, with $H_2$:$CO_2$ molar ratios of ~3 and low CO outlet concentrations. A performance comparison was performed with two other reforming substrates with the same catalyst formulation, namely, a conventional cordierite monolith and a conventional stainless steel microreactor. Results show for the Si-micromonolithic reactor a remarkable improvement of the specific hydrogen production rate (per unit reactor volume and feed flowrate), operating at considerably reduced residence times, due to the increase in contact area per unit volume.



## 1. Introduction

Hydrogen production technologies are currently being investigated and developed actively, motivated by the possible use of $H_2$ as energy carrier and the rapid implementation of fuel cells [1]. The proton Exchange Membrane Fuel Cell (PEM-FC) appears nowadays as the most promising for small-scale applications as it offers higher energy density, operation at lower temperature and with increased safety and lower cost when compared with other types of fuel cells [2]. The steam reforming of ethanol (eq. (1)) arises as an attractive solution for supplying hydrogen for PEM-FC feeding, while avoiding safety and storage issues related to other gaseous (hydrogen, methane) and liquid fuels (hydrogen, methanol). Moreover, ethanol is especially appealing as primary fuel for fuel processors since it can be easily obtained from renewable biomass and its use supposes an almost closed $CO_2$ cycle [3,4].

$$CH_3CH_2OH + 3H_2O \rightarrow 2CO_2 + 6H_2 \quad (1)$$

The rapidly growing market for power sources for new portable electronic devices moved researchers to investigate

* *Corresponding author*. Institut de Tècniques Energètiques, Universitat Politècnica de Catalunya, Diagonal 647, ed. ETSEIB, 08028 Barcelona, Spain. Tel.: +34934011708; fax: +34934017149.
E-mail addresses: e.lopez@upc.edu (E. López), jordi.llorca@upc.edu (J. Llorca).
0360-3199/$ – see front matter 
doi:10.1016/j.ijhydene.2010.01.146

in the development of miniaturized fuel cell systems [5], including hydrogen production facilities. Although considerable work has been performed on hydrogen production using packed bed reactors [4,6–8], they cannot be arbitrarily scaled down for practical implementation when a small-scale is required. In addition, the intended reactions show strong thermal effects and conventional fixed-bed reactors, containing randomly packed catalyst pellets, exhibit poor heat transfer characteristics [9,10]. Micro reactors address both problems of moving down the scale and increasing the heat transfer rates by the deposition of the catalyst directly on the reactor walls. The introduction of novel manufacture techniques permits the miniaturization of structures and the achievement of a remarkable increase of the specific contact area (i.e., specific heat/mass transfer rates). The small dimensions attained for the microchannels and their very high reproducibility open new possibilities for reaction control by achieving previously inaccessible residence times and flow pattern homogeneity [11]. Numerous micro-devices for hydrogen production and its posterior purification have been reported [5,12–15], with typical channel dimensions ranging from 100 to 500 μm. Nevertheless, further reductions of the $H_2$ generation scale are hardly attained by using the conventional geometries and/or manufacture techniques of existing microreactors. Therefore, breakthrough technologies which provide higher $H_2$ generation rates per unit volume and, at the same time, enable further downscaling are required.

Studies on photo-assisted electrochemical etching techniques applied to the fabrication of micromonolithic substrates have been recently reported. Lithographically pre-structured silicon wafers are used as source material [16–18]. Due to the very exciting properties of the achieved structures, many applications have been proposed in the fields of gas sensing [19,20], photonic crystals [21], absorbents [18] and biotechnology [22] among others. In Llorca et al. [23] we reported a successful procedure towards the deposition of a homogeneous and thin layer of catalyst on the channels walls of micromonolithic silicon substrates. Furthermore, we demonstrated the feasibility of conducting reforming reactions on them [23,24]. The present contribution addresses results regarding the design, manufacture and experimental proof of concept of an ethanol reformer for portable-fuel cell feeding profiting Si-micromonolithic substrates. Several Si wafers were functionalized with a Co catalyst and implemented in-series into a stainless steel casing with incorporated evaporation facilities for undiluted ethanol + water liquid feed. A parametric sensitivity analysis regarding temperature, feed concentration and load was performed to attain optimal operation windows.

## 2. Experimental method

### 2.1. Catalyst preparation

Photo-assisted electrochemical etching was carried out to prepare three silicon disks with straight, parallel channels of 3.3 μm in diameter. The substrate material was <100> *n*-type float-zone silicon. In the etching procedure, the pre-structured silicon wafers (by lithography, square arrange) were in contact with the electrolyte, while the backside was illuminated through an array of LEDs with an 880 nm peak emission wavelength. A constant anodic potential of 2 V was applied. After the growing of the channels, the pores were opened from the back side by removing the remaining silicon with 25 wt% tetramethylammonium hydroxide (TMAH) solution at 358 K. The resulting structures were silicon membranes with cylindrical pores (channels) opened at both sides and arranged in a square lattice with a periodicity of 4 μm. The excellent reproducibility and perfect cylindrical shape of the channels allow uniform flow distribution. Each micromonolith (~0.21 mm length, Ø16 mm) comprises ca. $8 \times 10^6$ channels, with a specific contact area of $4.1 \times 10^5$ $m^2$ $m^{-3}$. A pressure drop of only ca. 170 ± 10 Pa was measured with nitrogen flowing at 60 mL $min^{-1}$ and room temperature. The obtained micromonoliths also profit from the good thermal conductivity of silicon, its thermal stability and mechanic robustness. A SEM image of the achieved micromonolith is shown in Fig. 1. More details can be found elsewhere [23].

The silicon substrates described above were functionalized for ethanol steam reforming at moderate temperature (623–773 K) by direct coating using an *in-situ* route, as reported by Llorca et al. [23]. An alkaline-stabilized cobalt-based catalyst was used here exploiting its ability of reducing the usually high temperatures (773–973 K) required for C–C bond breaking [25]. A dimethylketone solution containing $Zn^{2+}$ and $Co^{2+}$ (0.35 M, equal amounts, nitrate precursors), $Na^+$ (0.07 M, nitrate precursor), and urea (1.4 M) was forced to pass through the macroporous silicon channels by applying a pressure gradient (75 ± 1 kPa) with a vacuum pump. After ensuring a complete wetting of the channel walls, the silicon membranes were heated first at 348 K for 3 h, then at 393 K for 15 h, and finally at 673 K for 2 h at 2.5 K $min^{-1}$. By this procedure, a ca. 100 nm-thick layer of $Co_3O_4$–ZnO catalyst doped with $Na^+$ was achieved on the channel walls.

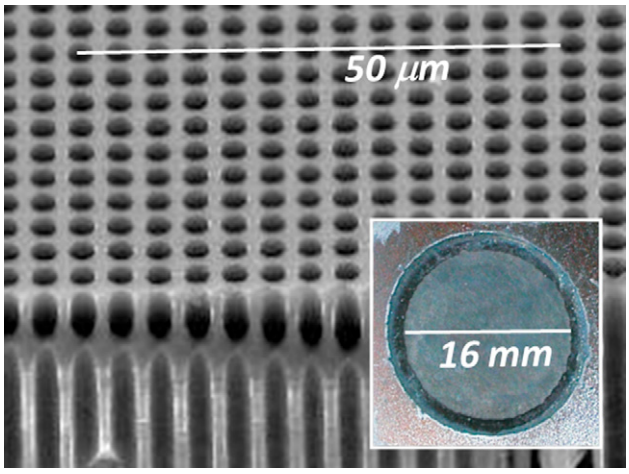


**Fig. 1 – SEM image of the channels of the silicon micromonolith. A complete silicon disk is shown by the conventional photograph of the lower-right corner.**

### 2.2. Reactor manufacture and implementation

The functionalized silicon micromonoliths were implemented in a microreactor machined in stainless steel in three differentiated sections: a) an evaporation/preheating section where four meandering microchannels provide a high contact area between the incoming feed (ethanol + water mixture) and the hot reactor body, b) a central section in which four 1/8″ diameter electric microcartridges are inserted to provide the necessary heat for evaporation and reaction, and c) a reaction chamber where the three silicon micromonoliths are placed in-series. Inlet/outlet conduits are welded to the first and third sections, respectively; adequate channels through the middle segment communicate the evaporation and reaction sections. Three 0.5 mm-diameter K-type thermocouples (±0.5 K) were placed in different zones of the reactor for temperature monitoring and control. Appropriate seals were implemented to avoid gas leakages and by-passes. The whole unit (three sections together) measures 40 × 40 × 19 mm. Fig. 2a shows a schematic representation of the achieved microreactor and Fig. 2b shows a photograph of the three sections.

The microreactor was thermally isolated with glass wool and ceramic materials and placed into an appropriate shell. The liquid feed mixture of ethanol and water was provided directly by a syringe pump (Genie Plus, Kent Scientific). After separation of condensable components, the gaseous products were analyzed by online gas chromatography (Agilent 3000A MicroGC, $<\pm 5\%$ in $y_j$) using MS 5 Å, PlotU and Stabilwax columns. Additionally, we measured the total volumetric flowrate of the dry outlet stream ($\pm 0.1$ mL min$^{-1}$). An electronic controller was used to govern the heating microcartridges and operate at the selected temperature level; a maximum allowable temperature of 773 K results from the microcartridges and the manufacturing method at hand. A uniform temperature distribution in the microreactor was checked. In addition, temperatures above 423 K were measured at all positions within the external shell, assuring no condensation of ethanol/water and reflux into the reactor.

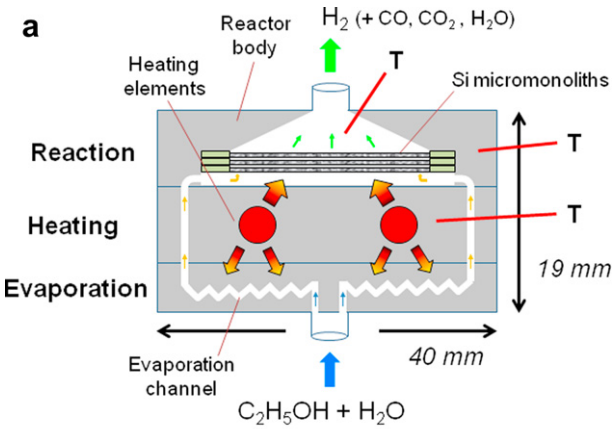


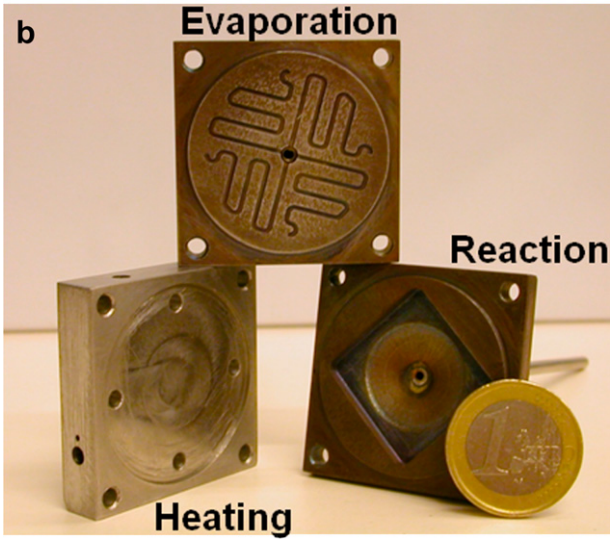


**Fig. 2 – (a) Schematic representation of the ethanol micro-reformer. (b): Photograph of the stainless steel machined sections of the microreactor. The rhombic cavity in the "reaction section" houses the silicon wafers; the circular section in the middle of it correspond to the area with channels in the wafers.**

### 2.3. Performance evaluation

Several experiments were conducted to study the steady-state performance of the functionalized micromonoliths and to find optimal operation windows. Feed concentrations at realistic conditions were selected, using non-diluted ethanol + water liquid mixtures at room temperature. The catalyst was treated prior to the experiments under flowing hydrogen (10% in He, 20 ml min$^{-1}$) at 723 K for 30 min. The experimental conditions explored are reported in Table 1.

The correct closure of the mass balance in the micro-reforming system was verified by measuring under steady-state conditions and in a precise period of time both the composition and flowrate of the gaseous outlet stream as well as the volume of liquid condensed from the reactor effluent. Operating conditions leading to complete ethanol conversion were selected here. Molar flowrates of the non-condensable components in the reactor effluent were calculated using the chromatographic analyses and total volumetric flowrate data (see Section 2.2). By closing element balances we were able to evaluate the ethanol conversion ($x_{EtOH}$), the volumetric hydrogen production rate ($V_{H_2}$) and the hydrogen yield ($\theta_{H_2}$) to quantify the micro-reformer performance.

As already reported in the literature [26–28], the reaction scheme reported below (eqs. (2)–(6)) applies to represent the ethanol steam reforming process over cobalt catalysts. It has been demonstrated that the simultaneous presence of metallic cobalt and cobalt oxide is required for the progress of the reaction. In fact, ethanol dehydrogenates into hydrogen and acetaldehyde (eq. (2)), which is further reformed with water to carbon monoxide (eq. (3)) and carbon dioxide (eq. (4)).

**Table 1 – Experimental conditions.**

| | |
|---|---|
| Temperature [K] | 673–773 |
| Pressure [bar] | 1 |
| $y_{H_2O^+}/y_{EtOH^+}$ | 3–13(1.5 < S/C < 6.5) |
| Load, $V_{liq^+}$ [ml min$^{-1}$, liquid] | 0.003–0.09 (0.0 < $\tau_{NPT}$ < 0.9 s) |

In addition, cobalt catalysts are active for the water-gas shift reaction (eq. (5)) at the selected temperature window. An undesired source of carbon monoxide and methane is the ethanol decomposition, as indicated by eq. (6).

$$CH_3CH_2OH \rightarrow CH_3CHO + H_2 \quad (2)$$

$$CH_3CHO + H_2O \rightarrow 2CO + 3H_2 \quad (3)$$

$$CH_3CHO + 3H_2O \rightarrow 2CO_2 + 5H_2 \quad (4)$$

$$CO + H_2O \leftrightarrow CO_2 + H_2 \quad (5)$$

$$CH_3CH_2OH \rightarrow CO + CH_4 + H_2 \quad (6)$$

Lack of blank activity of the reactor material (reactor body) towards ethanol conversion was checked by mounting the microreactor without the silicon micromonoliths and operating under the same feed concentration, reactor load and temperature. Moreover, in Llorca et al. [23], the reduced extent of the ethanol cracking reaction (eq. (6)) using a non-functionalized silicon micromonolith has been demonstrated.

## 3. Results and discussion

### 3.1. Influence of the operation temperature

Fig. 3 shows the influence of the operation temperature on the selectivity profile of the outlet gas stream for fixed feed conditions (flowrate and composition). The volumetric production rates of hydrogen ($V_{H_2}$), along with the corresponding ethanol conversions ($x_{EtOH}$), are also shown. As higher temperatures are selected, higher hydrogen and carbon dioxide molar fractions are achieved at the expense of the remaining gaseous compounds. This behavior points out

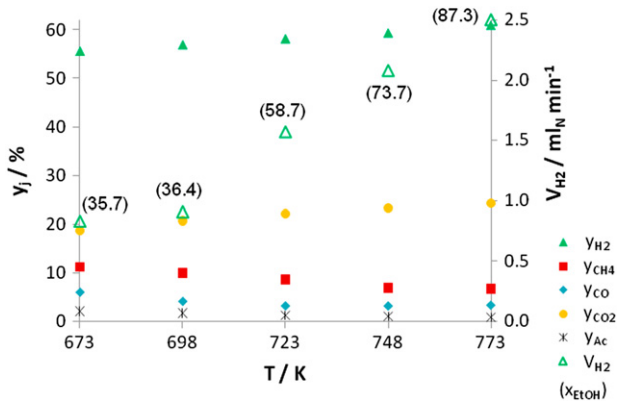


**Fig. 3 – Selectivity profiles ( $y_j$, closed symbols), hydrogen production rate ($V_{H_2}$, open symbols) and ethanol conversions ($x_{EtOH}$, between parentheses) for different operating temperatures. $V_{liq^+} = 0.00625$ $ml_{liq}$ $min^{-1}$ ($\tau_{NPT} = 0.44$ s), S/C = 3.**

the increasing predominance of reactions (2)–(4) over reaction (6) as the temperature is increased. At the essayed temperatures, the steam reforming of methane is almost negligible over the catalytic system used here [28]. In consequence, the extent of ethanol decomposition (eq. (6)) should be kept as low as possible to avoid an undesirable drop on the hydrogen yield. In fact, cobalt-based catalysts have been reported [26] to suppress methane-forming reactions (e.g., eq. (6)). Equilibrium calculations render values of 0.5% and 2.7% for $y_{CO}$ (dry basis) at 673 K and 773 K, respectively, whereas those for $CO_2$ amount 24.6% and 22.9% for the same temperatures. We measured outlet molar fractions of 6.1% and 3.3% (CO) and 18.7% and 24.2% ($CO_2$) at 673 K and 773 K, respectively. By comparing both equilibrium and measured data, the operation of the micro-reformer away from the equilibrium regarding the WGSR (eq. (5)) appears clear at 673 K. At 773 K, the measured $y_{CO}$ and $y_{CO_2}$ approach equilibrium values at a higher extent, although equilibrium is still not reached. Acetaldehyde molar fractions under 2% point out the outstanding ability of the selected catalyst towards acetaldehyde steam reforming [29,30].

Pronounced variations in the hydrogen production rate and ethanol conversion were measured for the selected range of operating temperatures. In fact, the volumetric hydrogen production rate ($V_{H_2}$) almost triplicates for a 100 K temperature variation, following the same qualitative pattern than that of the ethanol conversion. For the highest temperature of 773 K, with an almost 90% of ethanol conversion, a hydrogen yield (mol $H_2$ produced/mol ethanol fed) of 3 is achieved, with a $H_2/CO_2$ ratio of 2.5. A CO molar fraction slightly above 3% suggests the use of a shift reactor of reduced dimensions (or even neglect it) downstream the reformer, before feeding a final purification unit (e.g., a CO–PrOx reactor).

### 3.2. Influence of the load

A series of experiences varying the load of the liquid feed to the microreactor was performed to find out its influence on the reforming performance. Fig. 4 shows results regarding hydrogen flowrate, ethanol conversion and hydrogen yield for an operating temperature of 773 K and a water/ethanol molar ratio of 6 in the feed (S/C = 3). Complementary, Fig. 5 reports the outlet molar fractions for the product compounds measured by gas chromatography. Despite the appreciable increase of the outlet $H_2$ flowrate as the load is increased, the drop in residence time ($\tau$ shifts from 0.9 s to 0.05 s) reduces the ethanol conversion from complete to almost 50% and the hydrogen yield from 3.4 to 1.7 mol of $H_2$ produced per mol of ethanol introduced. As shown in Fig. 5, lower residence times result unfavorable for the extension of the water–gas shift reaction since an increase of $y_{CO}$ is observed while $CO_2$ contents decrease. Higher molar fractions of acetaldehyde are also measured for higher space velocities. Although complete ethanol conversion is achieved when low loads are selected, the competence between ethanol decomposition (eq. (6)) and ethanol dehydrogenation (and posterior reforming of acetaldehyde, eqs. (2)–(4)) becomes more appreciable, preventing a rise in hydrogen yield comparable to the rise in ethanol conversion (see Fig. 4). Regardless the previous remarks, a great robustness of the reforming unit towards the

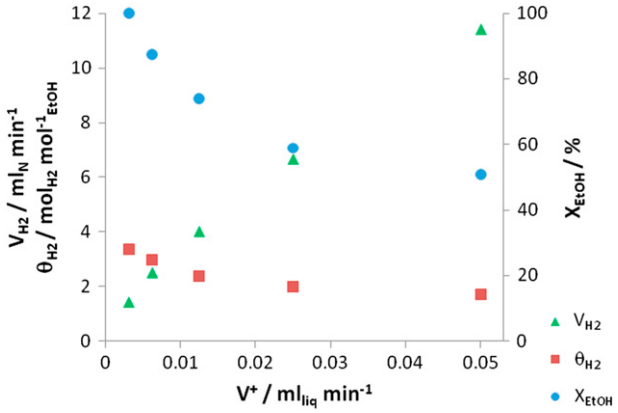


**Fig. 4 – Influence of the load on the hydrogen production rate ($V_{H_2}$), hydrogen yield ($\theta_{H_2}$) and ethanol conversion ($x_{EtOH}$) T = 773K, S/C = 3.**

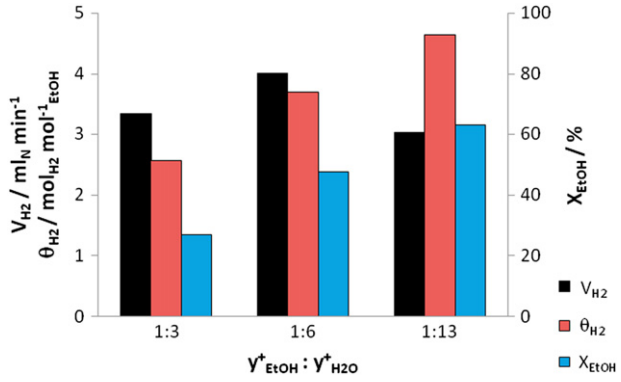


**Fig. 6 – Influence of the feed composition on the hydrogen production rate ($\theta_{H_2}$), hydrogen yield ($\theta_{H_2}$) and ethanol conversion ($x_{EtOH}$). T = 773K, $V_{liq^+}$ = 0.0125 $ml_{liq}$ $min^{-1}$ ($\tau_{NPT}$ ~ 0.2 s).**

reforming products, $H_2$ and $CO_2$, is observed for a 15-fold variation in the residence time.

### 3.3. *Influence of the feed composition (S/C ratio)*

Three different feed mixtures were selected for the operation of the micro-reformer. Along with the stoichiometric and bioethanol-like compositions (1:3 and 1:13 in ethanol:water molar ratios, respectively), we used an intermediate value with double excess of water as dictated by stoichiometry (1:6 ethanol:water). Fig. 6 reports hydrogen production, ethanol conversion and hydrogen yield for different inlet mixtures ethanol–water. If medium to high feed flowrates are used (as in Fig. 6), a clear beneficial effect is observed for mixtures with higher water contents regarding both ethanol conversion and hydrogen yield. However, a maximum is measured for the hydrogen production rate. In fact, mixtures with low S/C have high ethanol contents in the feed but attain poor conversions, whereas mixtures with high S/C convert adequately little amounts of ethanol (as most of the feed is water). Therefore, intermediate mixtures with ca. double excess water (S/C = 3) render higher hydrogen productions due to a more advantageous balance between ethanol

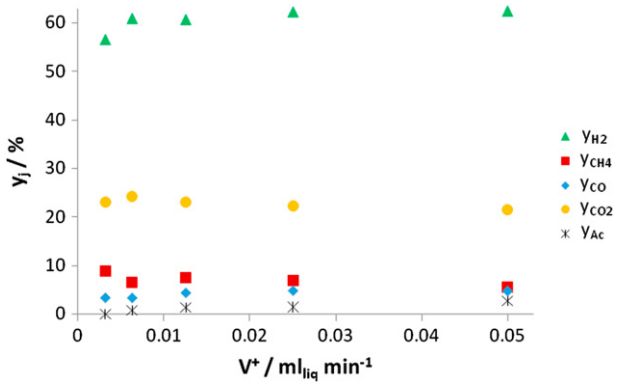


**Fig. 5 – Selectivity profiles at different load values. Experimental points correspond to data in Fig. 4.**

conversion and amount of ethanol available. If the reactor is operated with reduced feed flowrates, the residence time is high enough in all cases and no clear advantages in terms of conversion and yield are observed when selecting intermediate or bioethanol-like feed mixtures. In all cases (any feed flowrate), the operation with a stoichiometric mixture seems not recommendable as ethanol conversions are always lower and hydrogen yields reach only up to 1/3 of the maximum allowable of 6 (see eq (1)). From the measured selectivity profiles, appreciably higher molar fractions of acetaldehyde, carbon monoxide and methane point to adverse conditions for the reforming and water–gas shift reactions for S/C = 1.5. Moreover, water contents in feed higher than stoichiometric usually prevents coke formation as referenced elsewhere [31,32]. On the other hand, extremely diluted ethanol feeds (e.g., 1:13) are not recommended as higher amounts of energy are required for the excess water heating, evaporation and overheating (only partially recovered in the post-reactor condensation) as well as pumping power for the liquid feed. A moderated excess of water as the one used in this paper (S/C = 3) should be appropriate for the micro-reformer operation, providing suitable selectivity profiles while avoiding coke formation and reducing energy requirements.

Experiments fixing the ethanol feed flowrate were also performed for the three different mixture ratios (Table 1), resulting in noticeably differences in residence times. In fact, a 4-fold increase in space velocity when changing from a stoichiometric to a bioethanol mixture leads to a compensation effect. In particular, for an ethanol:water molar ratio of 1:3, poorer reforming conditions (i.e., less water) are balanced by larger residence times (and vice versa for mixtures 1:13). When extremely low inlet flowrates are selected, then the residence times are high enough as to render superior results for the bioethanol-like feed. In all other cases, a moderate excess water (1:6 in molar ratio) appears again as the preferred option.

### 3.4. *Long-term experiences*

Several long-term tests (15–24 h non-stop operation) were performed at T = 773 K, S/C = 3 and S/C = 6.5, and residence

times in the range 0.4–0.9 s. Results show remarkable constancy in selectivity profiles and hydrogen productivity. After more than 250 h operation no signs of catalyst deactivation were observed. However, the occurrence of carbon deposition was evidenced in the post-reacted silicon micromonoliths.

### 3.5. *Performance comparison with conventional monoliths and microreactors*

Although the same catalyst formulation was used, a straightforward comparison between performances of the silicon micromonolith and a conventional cordierite monolith is unviable as the different size of the supports prevents the use of exactly the same operating conditions. Nevertheless, we can use as a comparison basis an intensive measurement by normalizing performances by the volume of support and the injection load, as shown by eq. (7):

$$V_{H_2}^{sp}\left[\frac{Nml_{H_{2,g}}}{ml_{liq}.cm_R^3}\right] = \frac{V_{H_2}\left[\frac{Nml_{H_{2,g}}}{min}\right]}{V_{liq^+}\left[\frac{ml_{liq}}{min}\right]\cdot V_R[cm_R^3]} \quad (7)$$

In Fig. 7, the performance for both a conventional cordierite monolith [24] and the silicon micro-reformer are compared in terms of residence time ($\tau$) and specific hydrogen production rate ($V_{H_2}^{sp}$), both operating at a same ethanol conversion level of ca. 34% and with undiluted ethanol/water feed mixture (S/C = 3). The cylindrical cordierite monolith (400 cpsi) measures 18 mm in diameter by 18 mm length. As seen from Fig. 7, specific hydrogen productions of ca. 20-fold higher are attained in the Si-micromonolith at a residence time of 7-fold lower. Interestingly, almost the same product selectivity ($H_2$, $CH_4$, CO and $CO_2$) was measured for both systems. This increase in ($V_{H_2}^{sp}$) obeys to the dramatically superior contact area available in the silicon structure when compared to a ca. 1mm-channel cordierite monolith ($3.5 \times 10^5$ and $2.2 \times 10^3$ $m^2$ $m^{-3}$, respectively).

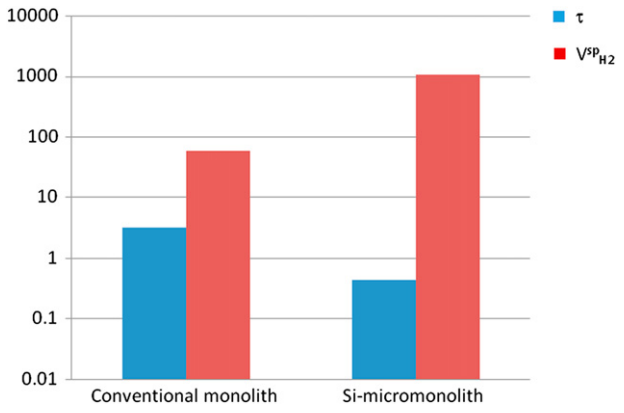


**Fig. 7 – Performance comparison between a conventional cordierite monolith (1 mm channel side, 18 mm diameter, 18 mm length) and the Si-micromonolithic reactor. $T$ = 673 K, $x_{EtOH}$ = 0.34, feed mixture = 1:6 ethanol:water molar. Conventional monolith: $V_{liq^+}$ = 0.1 $ml_{liq}$ $min^{-1}$, Si-micromonolithic reactor: $V_{liq^+}$ = 0.00625 $ml_{liq}$ $min^{-1}$.**

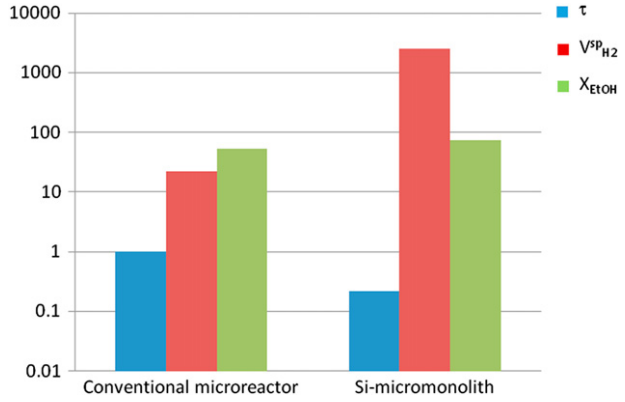


**Fig. 8 – Performance comparison between a conventional microreactor (13 78 mm-length channels, 0.5 mm channel equivalent diameter) and the Si-micromonolithic reactor. $T$ = 773 K, $V_{liq^+}$ = 0.0125 $ml_{liq}$ $min^{-1}$, feed mixture = 1:6 ethanol:water molar.**

A performance comparison of the silicon micromonolith with a conventional microreactor [14,24] was also performed. The microreactor had also the same catalyst formulation, deposited onto the walls of 13 semi-cylindrical channels of 0.7 mm diameter by 78 mm length. Fig. 8 shows residence times and specific hydrogen production rates (see eq. (7)) for both systems as well as ethanol conversion values. In this comparison scenario, the same feed flowrate was selected for both systems. The use of the silicon micromonolith led to an improvement in $V_{H_2}^{sp}$ of ca. 2 orders of magnitude operating at 1/5 of the residence time of the conventional microreactor and with ca. 20% increase in ethanol conversion. The selectivity distribution is again nearly the same for both the microreactor and the Si-micromonolith.

## 4. Conclusions

Micromonolithic silicon wafers, with ca. $8 \times 10^6$ channels (3.3 μm diameter and length/depth ca. 65), were functionalized with a $Co_3O_4$–ZnO catalyst doped with $Na^+$. Three wafers were implemented in-series inside a stainless steel casing, which included preheating/evaporation facilities and electrical microcartridges. The micro-reformer was successfully tested for ethanol steam reforming under non-diluted feed conditions. Typical selectivity distributions showed molar fractions of hydrogen and carbon dioxide in ratio of ca. 3 and CO molar fractions of 3–6% on a dry basis, with negligible quantities (<1%) of other by-products or intermediates (e.g., acetone, acetaldehyde, ethylene). Specific production rates exceeding 3.5 $l_N$ of $H_2$ per ml of liquid fed and $cm^3$ of micromonolith are possible due to the great geometric area of the substrate.

A parametric sensitivity study regarding operation temperature (673–773 K), feed concentration (S/C = 1.5, 3 and 6.5) and residence time (0.03–0.9 s) was performed to find optimal operation windows. A temperature level of ca. 773 K favored the reforming reaction over the ethanol decomposition and enhanced the extent of the water–gas shift reaction

(not in equilibrium for the selected residence times). Although a remarkable uniformity in the selectivity profiles was measured for the different loads tested, residence times in the range 0.4–0.9 s are preferred as they lead to almost complete ethanol conversion. A feed mixture of 1:6 ethanol:water (molar) presented a reasonable balance between reforming performance and not too-excessive energy demand.

The comparison of the reaction performance of the silicon micromonoliths (3.3 μm channels) with the performance of conventional cordierite monoliths (1 mm-channels) and conventional microreactors (~0.5 mm diameter equivalent), loaded with the same catalyst formulation, shows the tremendous advantages of increasing the geometric area per unit volume when reducing the working scale. In fact, Si-micromonoliths allow operation with highly reduced catalyst loads per unit reactor volume.

The studies conducted in the present contribution proved that microreforming technology based on functionalized silicon micromonoliths is technically viable, with superior performances when compared to conventional micro-reforming units. In addition, it can be easily scaled down (or up) according to the requirements of the process at hand. Therefore, Si-micromonoliths hold a promising future in on-site/on-demand hydrogen generation for portable applications.

## Acknowledgements

Technical assistance by Vicente Blasco is gratefully acknowledged. This work has been partially supported by projects CTQ2009-12520 and TEC2007-67081.

## Nomenclature

| | |
|---|---|
| S/C | steam-to-carbon ratio in feed |
| T | temperature, K |
| $V_{H_2}$ | hydrogen production rate, $Nml_{H_2} min^{-1}$ |
| $V^{sp}_{H_2}$ | specific hydrogen production rate (see eq. (7)), $Nml_{H_{2,g}} ml^{-1}_{liq}\ cm^{-3}_R$ |
| $V_{liq}$ | liquid flowrate, $ml_{liq}\ min^{-1}$ |
| $V_R$ | reactor volume, $cm^3_R$ |
| X | conversion |
| y+ | molar fraction feed |

*Subindex*

| | |
|---|---|
| Ac | acetaldehyde |
| EtOH | ethanol |
| g | gas |
| j | component j |
| $H_2O$ | water |
| liq | liquid (feed) |

*Greek letters*

| | |
|---|---|
| $\theta_{H_2}$ | hydrogen yield, mol hydrogen produced per mol ethanol in feed |
| $\tau$ | residence time (normal conditions), s |

## REFERENCES

[1] Brown LF. A comparative study of fuels for on-board hydrogen production for fuel-cell-powered automobiles. Int J Hyd Energy 2001;26:381–97.
[2] Song C. Fuel processing for low-temperature and high-temperature fuel cells: challenges, and opportunities for sustainable development in the 21st century. Catal Today 2002;77:17–49.
[3] Akande A, Aboudheir A, Idem R, Dalai A. Kinetic modeling of hydrogen production by the catalytic reforming of crude ethanol over a co-precipitated Ni–$Al_2O_3$ catalyst in a packed bed tubular reactor. Int J Hyd Energy 2006;31:1707–15.
[4] Ni M, Leung YC, Leung MKH. A review on reforming bio-ethanol for hydrogen production. Int J Hyd Energy 2007;32:3238–47.
[5] Kawamura Y, Ogura N, Yamamoto T, Igarashi A. A miniaturized methanol reformer with Si-based microreactor for a small PEMFC. Chem Eng Sci 2006;61:1092–101.
[6] Vaidya PD, Rodrigues AE. Insight into steam reforming of ethanol to produce hydrogen for fuel cells. Chem Eng J 2006;117:39–49.
[7] Haryanto A, Fernando S, Murali N, Adhikari S. Current status of hydrogen production techniques by steam reforming of ethanol: a review. Energy and Fuels 2005;19:2098–106.
[8] Navarro RM, Peña MA, Fierro JLG. Hydrogen production reactions from carbon feedstocks: fossils fuels and biomass. Chem Rev 2007;107:3952–91.
[9] Daszkowski T, Eigenberger G. A reevaluation of fluid flow, heat transfer and chemical reaction in catalyst filled tubes. Chem Eng Sci 1992;47(9–11):2245–50.
[10] Tsotsas E. Wärmeleitung und dispersion in durchströmten Schüttungen. 8th ed. VDI Düsseldorf: VDI-Wärmeatlas; 1998.
[11] Ehrfeld W, Hessel V, Löwe H. Microreactors-new technology for modern chemistry. Weinheim: Wiley–VCH; 2000.
[12] Kolb G, Hessel V. Micro-structured reactors for gas phase reactions. Chem Eng J 2004;98:1–38.
[13] Palo DR, Dagle RA, Holladay JD. Methanol steam reforming for hydrogen production. Chem Rev 2007;107:3992–4021.
[14] Casanovas A, Saint-Gerons M, Griffon F, Llorca J. Autothermal generation of hydrogen from ethanol in a microreactor. Int J Hyd Energy 2008;33:1827–33.
[15] Kolb G, Hessel V, Cominos V, Hofmann C, Löwe H, Nikolaidis G, et al. Selective oxidations in micro-structured catalytic reactors—for gas-phase reactions and specifically for fuel processing for fuel cells. Catal Today 2007;120(1):2–20.
[16] Lehmann V, Foell H. Formation mechanism and properties of electrochemically etched trenches in n-type silicon. J Electrochem Soc 1990;137:653–9.
[17] A. Rodriguez, T. Trifonov, R. Alcubilla, J. Llorca, A. Casanovas, A. Urbitzondo, M.P. Pina, J. Santamaria, P200800919 (25/03/2008, Spain).
[18] Urbiztondo M, Valera E, Trifonov T, Alcubilla R, Irusta S, Pina MP, et al. Development of microstructured zeolite films as highly accessible catalytic coatings for microreactors. J Catal 2007;250:190–4.
[19] Betty CA, Lal R, Sharma DK, Yakhmi JV, Mittal JP. Macroporous silicon based capacitive affinity sensor-fabrication and electrochemical studies. Sens Actuators B: Chem 2004;97:334–43.
[20] Kurowski A, Schultze JW, Lueth H, Schoening MJ. Micro and nanopatterning of sensor chips by means of macroporous silicon. Sens Actuators B: Chem 2002;83:123–8.

[21] Wehrspohn RB, Schilling J. A model system for photonic crystals: macroporous silicon. Phys Stat Sol A 2003;197: 673–87.
[22] Letant SE, Hart BR, van Buuren AW, Terminello LJ. Functionalized silicon membranes for selective bio-organism capture. Nat Mat 2003;2:391–5.
[23] Llorca J, Casanovas A, Trifonov T, Rodriguez A, Alcubilla R. First use of macroporous silicon loaded with catalyst film for a chemical reaction: a microreformer for producing hydrogen from ethanol steam reforming. J Catal 2008;255: 228–33.
[24] Casanovas A, Dominguez M, Ledesma C, Lopez E, Llorca J. Catalytic walls and micro-devices for generating hydrogen by low temperature steam reforming of ethanol. Catal Today 2009;143:32–7.
[25] Llorca J, Homs N, Sales J, Fierro JLG, Ramirez de la Piscina P. Effect of sodium addition on the performance of Co–ZnO-based catalysts for hydrogen production from bioethanol. J Catal 2004;222:470–80.
[26] Torres JA, Llorca J, Casanovas A, Dominguez M, Salvado J, Montané D. Steam reforming of ethanol at moderate temperature: multifactorial design analysis of Ni/$La_2O_3$–$Al_2O_3$, and Fe- and Mn-promoted Co/ZnO catalysts. J Pow Sources 2007;169:158–66.
[27] Dominguez M, Taboada E, Molins E, Llorca J. Co–$SiO_2$ aerogel-coated catalytic walls for the generation of hydrogen. Catal Today 2008;138(3–4):193–7.
[28] Casanovas A, de Leitenburg C, Trovarelli A, Llorca J. Catalytic monoliths for ethanol steam reforming. Catal Today 2008; 138(3–4):187–92.
[29] Llorca J, Ramirez de la Piscina P, Dalmon N, Homs N. Transformation of $Co_3O_4$ during ethanol steam-reforming. activation process for hydrogen production. Chem Materials 2004;16:3573–8.
[30] García V, Lopez E, Serra M, Llorca J. Dynamic modeling of a three-stage low-temperature ethanol reformer for fuel cell application. J Pow Sources 2009;192(1):208–15.
[31] Comas J, Mariño F, Laborde M, Amadeo N. Bio-ethanol steam reforming on Ni/$Al_2O_3$ catalyst. Chem Eng J 2004;98:61–8.
[32] Fatsikostas AN, Verykios XE. Reaction network of steam reforming of ethanol over Ni-based catalysts,. J Catal 2004; 225:439–52.